JSS Focus Issue on Thermoelectric Materials & Devices

# Peltier Supercooling with Isosceles Current Pulses: A Response Surface Perspective

**Alfred J. Piggott**[a,b,z] **and Jeffrey S. Allen**[a,*]

[a]*Michigan Technological University, Houghton, Michigan 49931, USA*
[b]*Applied Thermoelectric Solutions LLC, Novi, Michigan, USA*

Using a pulsed electrical current enables a temporary state in which a Peltier element achieves temperatures below that obtained with a steady current. This is referred to as supercooling. Supercooling is followed by a period of superheating during which Peltier heat transfer is diminished and the surface temperatures increases. Most studies have found that the duration of superheating is longer than the duration of supercooling. As a result, the current pulse generates a net heating instead of enhanced cooling. There are limited studies that have shown the possibility of net cooling during a current pulse. The objective of this paper is to discuss the operating conditions for which net cooling is possible and maximized. The interaction between pulse duration and pulse height using isosceles shaped current pulses on net cooling was investigated using response surfaces generated using electrical-thermal analogies in SPICE. Pulse duration ranged from 0.1 to 10.0 seconds and pulse height ranging from 1.01 to 6.0 times steady current. Response surfaces were used to map a variety of performance factors; including the transient time to achieve a minimum temperature, the pulse cooling enhancement, transient penalty and transient advantage. The optimal combination of pulse duration and pulse height was identified.
© The Author(s) 2017. Published by ECS. This is an open access article distributed under the terms of the Creative Commons Attribution 4.0 License (CC BY, http://creativecommons.org/licenses/by/4.0/), which permits unrestricted reuse of the work in any medium, provided the original work is properly cited. [DOI: 10.1149/2.0061703jss] All rights reserved.

Manuscript submitted August 17, 2016; revised manuscript received December 5, 2016. Published January 14, 2017. *This paper is part of the JSS Focus Issue on Thermoelectric Materials & Devices: Phonon Engineering, Advanced Materials and Thermal Transport.*

The cooling requirements for electronic devices has and continues to increase in response to higher power densities and smaller packaging.[1] Peltier devices offer a convenient method of 'pumping' heat. Peltier coolers are solid state heat pumps that directly convert electric current to a temperature difference and heat flux. Imposing a temperature difference will induce a current flow. The operating principle utilized is the thermoelectric effect.

Advantages of utilizing thermoelectrics for thermal management include heating and cooling from the same device, precise temperature control within 0.01°C,[2] ability to cool to temperatures below ambient, COP greater than one when using the device for heating, site specific thermal management rather than cooling the entire enclosure, no moving parts, high reliability, silent operation, operation in any orientation, no fluorocarbon usage and high cooling power density.

These devices have many commercial thermal management applications including electronics and CPU cooling applications.[3] Thermoelectric air conditioners maintain enclosure temperatures for many different industries like hazardous environment, telecommunications, military, laboratory, and outdoor kiosk.[4] Home and office products include small refrigerators,[5] mattresses[6] and office chairs.[7] These devices are also used in medical products that provide thermal therapy.[8] Automotive applications include temperature controlled seating,[9] cup holders and mini in-vehicle refrigerators.[10] Recent research has focused on use of these devices for hybrid vehicle battery thermal management systems[11,12] and zonal heating and cooling of passenger vehicles.[13]

Equation 1 is the governing differential equation[14] for a single free-standing thermoelement under transient conditions. The assumptions are one-dimensional heat transfer and constant material properties. Here $I$ is the electrical current flowing parallel to the dimension $L$ and perpendicular to the area $A$. The distribution of temperature at any location $x$ and time $t$ is described as $T(x,t)$. In this equation $\rho$ is the electrical resistivity, $\kappa$ is the thermal conductivity and $a$ is the thermal diffusivity.

$$\frac{\partial^2 T(x,t)}{\partial x^2} + \frac{I^2\rho}{A^2\kappa} = \frac{1}{a}\frac{\partial T(x,t)}{\partial T} \qquad [1]$$

Typical boundary conditions applied to Equation 1 are constant temperature on the hot side and constant flux from Peltier cooling on the cold side. Here $\alpha = \alpha_p - \alpha_n$ and $I$ is current.

$$T(x = L, t) = T_h \qquad [2]$$

$$\left.\frac{\partial T(x,t)}{\partial x}\right|_{x=0} = \frac{\alpha I T_c(t)}{A\kappa} \qquad [3]$$

Analytical approximations and numerical solutions have been developed for this set of equations.[14–16]

In contrast to transient conditions, steady state cooling power at $T_c$ for $n$ couples is expressed as

$$\dot{Q}_c = n\left[\alpha T_c I - \left(\frac{1}{2}\right) I^2 R - K\Delta T\right] \qquad [4]$$

This equation is made up of a Peltier cooling term, a Joule heating term and a Fourier conduction term. Here $\alpha$ is the Seebeck coefficient of the couple $\alpha = \alpha_p - \alpha_n$ [V/K], $T_c$ is the temperature of the cold side of each thermoelement, and $I$ is the electric current through the couple. $R$ is the electrical resistance of the couple in units of ohms. $K$ is the thermal conductance [W/K] of the couple and $\Delta T$ is the temperature difference between $T_c$ and $T_h$. The resistance $R$ is dependent on the thermoelement material electrical resistivity $\rho$ and the thermal conductance $K$ is dependent on the thermoelement material thermal conductivity $k$. Increasing $\alpha$ while decreasing $\rho$ and $k$ lead to improved cooling power, $\dot{Q}_c$. Thermoelectric materials are likewise characterized with the figure of merit, $Z = \alpha^2/\rho k$. Here $\alpha$ is the Seebeck coefficient and can be $\alpha_p$ or $\alpha_n$. Increasing $Z$ leads to improved performance.

Two values of electric current are of interest for this work. $I_{\max}$ is the electrical current that sustains the maximum temperature difference between $T_h$ and $T_c$. $I_{opt}$ is the electrical current that sustains maximum $\dot{Q}_c$. $I_{\max}$[17] and $I_{opt}$[18] are characterized as follows:

$$I_{\max} = \frac{\alpha}{R}\left[\left(T_h + \frac{1}{Z}\right)^2 - T_h^2\right]^{1/2} - \frac{1}{Z} \qquad [5]$$

*Electrochemical Society Member.
[z]E-mail: Alfred@ThermoelectricSolutions.com

Redistribution subject to ECS terms of use (see ecsdl.org/site/terms_use) unless CC License in place (see abstract).

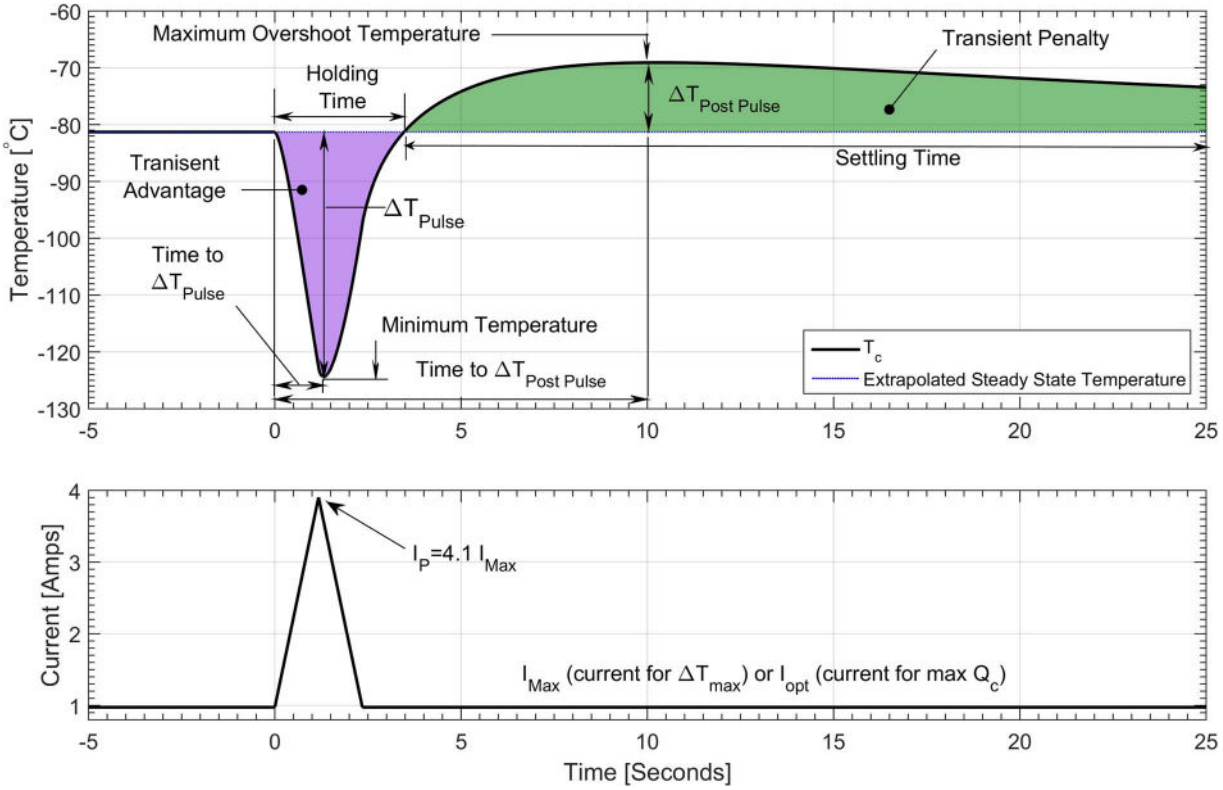


**Figure 1.** Performance factors and temperature response following a triangle current pulse.

$$I_{\text{opt}} = \frac{\alpha T_h}{R} \quad [6]$$

Here $\alpha = \alpha_p - \alpha_n$ [V/K] is the Seebeck coefficient of the couple and $R$ is the electrical resistance of the couple.

In contrast to steady state electrical current operation described above, research of pulsed supercooling operation consists of investigating the effects of current pulses on device performance. These pulses are applied while the device is operating at steady current.

Figure 1 illustrates the effect of such a current pulse while operating at $I_{max}$ steady current. Upon application of a current pulse, an instantaneous lower temperature (supercooling) is achieved. $T_c$ decreases to a minimum and then rises above the steady state ($I_{max}$) value to a maximum. Then $T_c$ decreases exponentially to the steady-state value. This instant lower temperature achieved followed by an overshoot is due to different time constants of Peltier cooling and Joule heating. Increased Peltier cooling is an instantaneous and interfacial effect that only takes place at the cold junction of each couple. Joule heating takes place instantly throughout the volume of each thermoelement. The volumetric Joule heat has a slower time constant and is delayed from reaching $T_c$ by diffusion throughout the thermoelement.

The following nomenclature, described in Figure 1 will be used for this work: $\Delta T_{pulse}$,[15] $\Delta T_{postpulse}$,[15] holding time,[19] time to minimum temperature,[20] time to maximum temperature overshoot,[21] settling time,[22] transient advantage,[19] transient penalty,[19] net transient advantage,[21] and pulse cooling enhancement.[19]

Variables that affect pulsed Peltier cooling include: thermoelement length,[15] current pulse amplitude[15,19] pulse duration,[19] pulse shape,[14,16,19,22–27] time between pulses,[28] thermoelectric figure of merit,[15] thermoelement thermal diffusivity [15], thermoelement shape[29–31] and the number of stages of a multi-stage thermoelectric cooler.[32] Of these variables, there are only two that can be varied to change the operating conditions for any given pulse shape. These two are pulse height, $P = I_{\text{pulse}}/I_{\text{max}}$ [15] and pulse duration.

Manno et al.[19] first defined the metrics transient advantage and transient penalty. For the constant pulse height and pulse duration simulated, Manno et al.[19] found for an Isosceles shaped pulse, the transient advantage was larger than the transient penalty. This research for the first time quantified that it is possible to have a net cooling advantage with transient operation. Since the operating parameters chosen for this study may have been incidental, the possibility of another combination of pulse height and pulse duration where the transient advantage is even larger than transient penalty is likely to exist.

The range of operating conditions for which transient advantage is larger than transient penalty for an Isosceles shaped current pulse has been identified herein. Response surfaces of net transient advantage[21] as a function of pulse height and pulse duration over a comprehensive range for each variable are developed. Furthermore the effects to other characteristic transient parameters shown in Figure 1 have been examined, with a surface generated for each parameter over the same comprehensive range of pulse height and pulse duration. Finally the effects of starting the pulses from two different steady state currents ($I_{max}$ and $I_{opt}$) are discussed.

This research is an important step toward achieving the iNEMI road map goal of finding cost effective and more effective solutions by maximizing performance of a given device and understanding the tradeoffs of improved performance with other characteristic transient parameters. Increased transient performance would allow a device to be downsized at lower cost or improve performance at the same cost.

## Materials and Methods

The object of the study was a single freestanding thermocouple as shown in Figure 2. The model was originally developed by Mitrani et al.[14] The height of the thermoelement was 5 mm with a cross sectional area was 1 mm$^2$.[14] Material properties of $Bi_2Te_3$ were used. For the generated surfaces, $\sigma = 1.0482e^5\ \Omega^{-1}\ m^{-1}$,

Redistribution subject to ECS terms of use (see ecsdl.org/site/terms_use) unless CC License in place (see abstract).

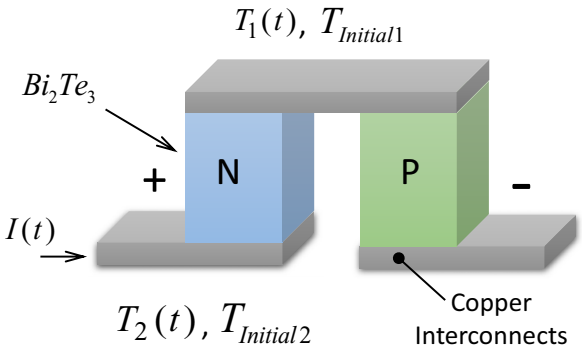


**Figure 2.** Thermocouple.

**Table I. Thermal Electrical Analogies.**

| Thermal Quantity | Electrical Analogy |
|---|---|
| Temperature [K] | Voltage [V] |
| Absolute Zero [0 K] | Ground [0 V] |
| Thermal Energy Flow Rate, $\dot{Q} = \left(\frac{\Delta T}{R_{th}}\right)[W]$ | Current Flow, $I = \left(\frac{\Delta V}{R}\right)[A]$ |
| Thermal Energy, $Q = \left(\frac{\Delta T t}{R_{th}}\right)[J]$ | Charge, $C = \left(\frac{\Delta V t}{R}\right)[As]$ |
| Thermal Conductivity, $k[\left(\frac{W}{mK}\right)]$ | Electrical Conductivity, $\sigma[\left(\frac{1}{\Omega m}\right)]$ |
| Thermal Mass, $C_{th}[\left(\frac{J}{K}\right)]$ | Electrical Capacitance, $C = \left(\frac{As}{V}\right)[F]$ |
| Thermal Resistance, $R_{th}[\left(\frac{K}{W}\right)]$ | Electrical Resistance, $R = \left(\frac{V}{I}\right)[\Omega]$ |

$\kappa = 1.5718\,Wm^{-1}\,K^{-1}$, $\alpha = 1.9700e^{-4}\,V\,K^{-1}$, $\rho = 7530\,kg\,m^{-3}$, $c_p = 544\,J\,kg^{-1}\,K^{-1}$.[33] These material properties were found by interpolating between data given at multiple temperatures. This interpolation used a sixth order polynominal curve fit to 308.15 K. The thermoelectric figure of merit was, $ZT_h = 0.89$. $T_h$ was maintained at 308.15 K. The steady state currents used prior to pulsing were $I_{max}$=0.9748 amps and $I_{opt}$=1.272 amps. The independent variables were pulse duration, which ranged from 0.1–10 seconds and pulse height $P = I_P/I_{\max}$ or $P = I_P/I_{\text{opt}}$ which ranged from 1.01 to 6 times the steady current. The pulse shape was an Isosceles triangle.

Differential equations derived for transient thermoelectric operation are unable to be solved in closed form,[14] therefore other solution methods are used. Snyder et al.[15] derived a 1D linear approximation model of a couple that was capable or modeling the supercooling portion of a transient pulse event. Three dimensional models that use ANSYS[34] or Comsol[35] have been used to model the entire event but these models are computationally complex. For this work, a transient model was developed in SPICE. SPICE was chosen because it was expandable for future studies in terms of adding mass, boundary conditions and thermal interface resistances. Furthermore the software is free, accurate and fast. The speed was beneficial due to the large number of simulations required to generate the response surfaces.

In the 1970's, SPICE (Simulation Program with Integrated Circuit Emphasis) was developed[36] for solving integrated circuit problems. SPICE solvers can also be used to solve electrical-thermal analogy problems. SPICE analogy models have been developed to simulate thermoelectric coolers. Chavez et al.[37] designed a steady state SPICE model of thermoelectric cooler that was accurate to within 0.5°C. Lin[38] created a steady state SPICE model designed to accept inputs from thermoelectric cooler manufacture data sheets with very good accuracy. Lineykin and Ben-Yaakov[18] developed a semi-lumped/semi-distributed mass transient SPICE model. Mitrani et al.[14] devised a 1D distributed mass model suitable for simulating transient pulsed cooling using SPICE. In this model, there was good agreement with other models[14] and this model is the basis of the work herein. Sullivan et al.[39] compared his SPICE model results with a finite volume Fluent model. There was good agreement of results between the two models, however the SPICE model was up to 430% faster.

The Mitrani et al.[14] model utilized for this study is a scalable 1D model of a thermoelectric couple and is made up of both a thermal and electric portion. Each portion consists of networked electrical components and is solved using software that contains a SPICE algorithm. For the thermal model, electrical-thermal analogies were used (shown in Table I) to decide the input values for each electrical components. The electrical-thermal analogy portion and the pure electrical circuit portion are linked to capture the combined electrical and thermal nature of a device. The physics associated with the thermoelectric device including Peltier cooling, Peltier heating, Joule heating, thermal resistance, thermal capacitance, electrical resistance and Seebeck voltage. The model takes a distributed mass and heat generation approach and captures the time separation between the Peltier effect, Joule heating effect, the Seebeck effect and transient thermal conduction throughout the thermoelement. The thermoelement is broken down into discreet parts that are analogous to finite elements. With this model, fifty finite elements are used.

In the thermal portion of the model, each finite element has mass, internal Joule heat generation and thermal resistance. Here, mass is analogous to a capacitor. Joule heat generation is analogous to current flow in a current source. Thermal resistance is analogous to electrical resistance. The Peltier effect is a heat flow and is analogous to current flow in a current source. Current out of a node simulates Peltier cooling and current into a node simulates Peltier heating. A diagram of the circuit analogy is available.[14]

The electrical model consists of a separate circuit on the same schematic as the thermal analogy model. Both of these models are solved simultaneously. The electrical model contains one current source. This is where the input electrical current for the model is defined. The electrical circuit also contains a voltage source and resistor for each finite element of the model. These voltage sources simulate the Seebeck voltage generated at each finite element in the thermal analogy model. The voltage sources are software linked to the thermal model and are dependent on the temperature difference across each finite element of the thermoelement model multiplied by the Seebeck coefficient. The resistors in the electrical model simulate the electrical resistance of each finite element of the thermoelement.

A voltage source is connected to the hot side of the device as a boundary condition. The voltage source in this model acts as a constant temperature thermal reservoir that maintains the hot side temperature.

The solve procedure for SPICE starts with the program forming a set of equations for each node of the circuit using Kirchhoff's current law (KCL). The matrix of equations is then solved by Gaussian elimination. When voltage sources are used in place of current sources, the voltage matrix is not known and therefore Gaussian elimination cannot be used. In this case, SPICE first uses a Norton equivalent circuit and then solves the matrix with Gaussian elimination. For circuits with nonlinear elements, the Newton-Raphson method is applied followed by Gaussian elimination. For transient simulations, SPICE utilizes numerical integration.[40]

The modeling process is categorized into four main steps. The first step is the model build step. This is the step where the model is built with the SPICE software. The second step is the preprocessing step. Here, the inputs to the SPICE model are calculated and entered into the SPICE model. This includes all variables for all electrical components and the PWL (Piece-wise Linear) electrical current text file which dictates the electrical current profile used. The third step is running the SPICE model and exporting the data. This can be done manually or by using a third party automation software. The fourth step is post processing the exported data. A detailed explanation of this process is available.[21]

The response surfaces generated required 2025 combinations of pulse-height and pulse duration to be simulated. This means 2025 PWL electrical current profile files for each surface. Generating these PWL files manually as well as post processing would have been time

Redistribution subject to ECS terms of use (see ecsdl.org/site/terms_use) unless CC License in place (see abstract).

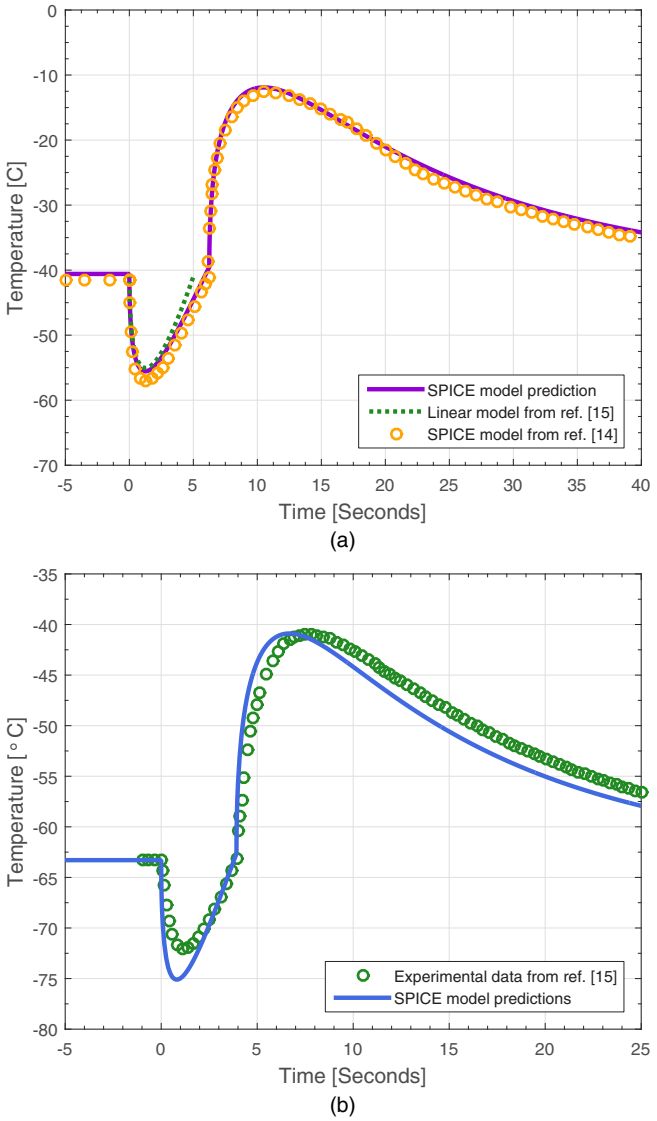


**Figure 3.** SPICE model validation (a) SPICE model prediction compared with other models (b) SPICE model prediction compared with experimental data.

prohibitive so the calculations and post processing of these files was automated using nested loops.

***Model validation.—***The SPICE model used herein was validated in two ways. The first method of validation was a comparison of the model predictions with other available models. The second method of validation was a comparison with the predictions of the model with experimental data.

The SPICE model is compared to the results from a linear model shown in Equation 7,[15]

$$\frac{T(x,t)-T_{ss}}{z(T_c)^2} = (P^2-1)\frac{at}{L^2} - (P-1)\frac{\sqrt{at}}{L}\mathrm{e}^{-x/\sqrt{at}} \qquad [7]$$

where $T_{ss}$ is the steady state temperature profile corresponding to $\Delta T_{max}$, $T_c$ is the temperature prior to the current pulse, $P = I_p/I_{\max}$, $a$ is the thermal diffusivity, and $L$ is the length of the thermoelectric element parallel to current flow. There is good agreement between the SPICE model and this linear model with the same properties as shown in Figure 3a, though the linear model cannot capture the transient penalty region. A second model is also used as a comparison. This model, developed by Mitrani et al.,[14] is also coded into SPICE. There are slight differences between the two SPICE models due to uncertainty in material properties. The source for the temperature dependent material properties was reported by Mitrani et al.,[14] but not the specific values used. The uncertainty lies in the interpolation between temperatures for the reported values.

To determine the exact properties used by Mitrani et al.,[14] one would need to know the original temperature and the type of curve fitting that was used. To extract the material properties from the table for the model validation herein, constant temperature properties were used as determined at the steady state temperature $T_{ave} = (T_h + T_c)/2 = 266.15\,K$. A second order curve fit was used for α, a first order for σ, and fourth order for κ. The properties and other input data used herein are $\kappa = 1.9045\,e^{-4}\,V\,K^{-1}$, $\sigma = 1.1321\,e^{5}\,\Omega^{-1}m^{-1}$, $\kappa = 1.6468\,W\,m^{-1}K^{-1}$, $\rho = 7530\,kg\,m^{-3}$, $c_p = 544\,J\,kg^{-1}K^{-1}$, $T_c = 232.15\,K$, $\Delta T_{max} = T_h - T_c = 68\,K$ at $\dot{Q}_c = 0$, $I_{max} = 0.977\,A$, $I_p/I_{max} = 2.5$, Pulse duration $= 6.245\,sec$, $L = 5\,mm$, $A = 1\,mm^2$. The source of the intrinsic thermoelement properties is a Melcor handbook[41] that is no longer publicly available. The fitted equations for this material data as a function of temperature in $K$ can be found below in Equations 8–10. These equations are valid from 225 K to 475 K.

$$\alpha(T) = -2.02518\,e^{-9}T^2 + 1.42345\,e^{-6}T - 4.49536\,e^{-5}\ \frac{V}{K} \qquad [8]$$

$$\rho(T) = 4.35357\,e^{-8}T - 2.75414\,e^{-6}\,\Omega\,m \qquad [9]$$

$$\kappa(T) = 3.46200\,e^{-10}T^4 - 4.88458\,e^{-7}T^3 + 2.82165\,e^{-4}T^2 - 7.65339\,e^{-2}T + 9.50065\ \frac{W}{m\,K} \qquad [10]$$

The second method used to validate the model used herein was by comparison with experimental data in Figure 3b. Intrinsic material properties were provided in a paper subsequent to the experimental data.[16] The properties and parameters provided were $\alpha = 2.35\,e^{-4}\,V\,K^{-1}$, $\kappa = 1.2\,w\,m^{-1}\,K^{-1}$, $\sigma = 5.1100\,e^{4}\,\Omega^{-1}\,m^{-1}$, $\rho c_p = 1.20e6\,J\,m^{-3}\,K^{-1}$, $A = 1.0\,e^{-6}m^2$, $L = 0.0058\,m$, $T_c = 209.86\,K$, $I_{max} = 0.675$ at $\dot{Q}_c = 0$, $\tau = 4\,sec$, $I_p/I_{max} = 2.5$, $ZT_c = 0.51$ at $T_c = 229.85\,K$. The intrinsic material properties could not be used to accurately reproduce the characteristic supercooling transient because the measurement location for the experimental results is not provided. The unavailable items were temperature dependent thermoelement properties, hot side thermal interface resistance to the heat sink, heat sink thermal resistance, cooling rate for an actively cooled heat sink and mass of the heat sink.

Instead of using intrinsic properties to reproduce the experimental data, effective properties were used. These effective properties can be calculated knowing the steady state parameters $I_{max}$, $\Delta T_{max}$, $T_h$, $Q_{max}$, $A$, and $L$.[17] The effective material properties take into account electrical and thermal contact resistances, steady state temperature dependence of the material and steady state convective and radiative losses. These properties are specific to the system and the provided intrinsic properties are specific to the thermoelement.

The process to find the effective properties was to first find the dimensional figure of merit, $z$. This was found from the provided $zT_c$ and associated temperature. The dimensional figure of merit was lower than that found with the intrinsic properties. This was acceptable and expected because it was calculated with system level data and therefore represents an effective property that takes into account losses. Next $\Delta T_{max} = T_h - T_c = Z(T_c)^2/2$ [15] and $T_h$ were determined. $Q_{max}$ was not provided and can be calculated with $Q_{max} = \alpha^2 T_c^2/2R$ [3] where α is the Seebeck coefficient of the couple, $\alpha = \alpha_p - \alpha_n = (I_{max}/T_h - \Delta T_{max})R$ [17] where R is the electrical resistance of the couple. In the resulting equation, R could not be determined with effective properties. $R$ was found iteratively when the output of the SPICE model converged as best as possible with the experimental data. The effective properties that were used to generate the SPICE model output in Figure 3b are $\alpha^* = 1.3077\,e^{-4}\,V\,K^{-1}$, $\kappa^* = 1.0374\,w\,m^{-1}\,K^{-1}$, $\sigma^* = 1.4265\,e^{5}\,\Omega^{-1}\,m^{-1}$.

Redistribution subject to ECS terms of use (see **ecsdl.org/site/terms_use**) unless CC License in place (see abstract).

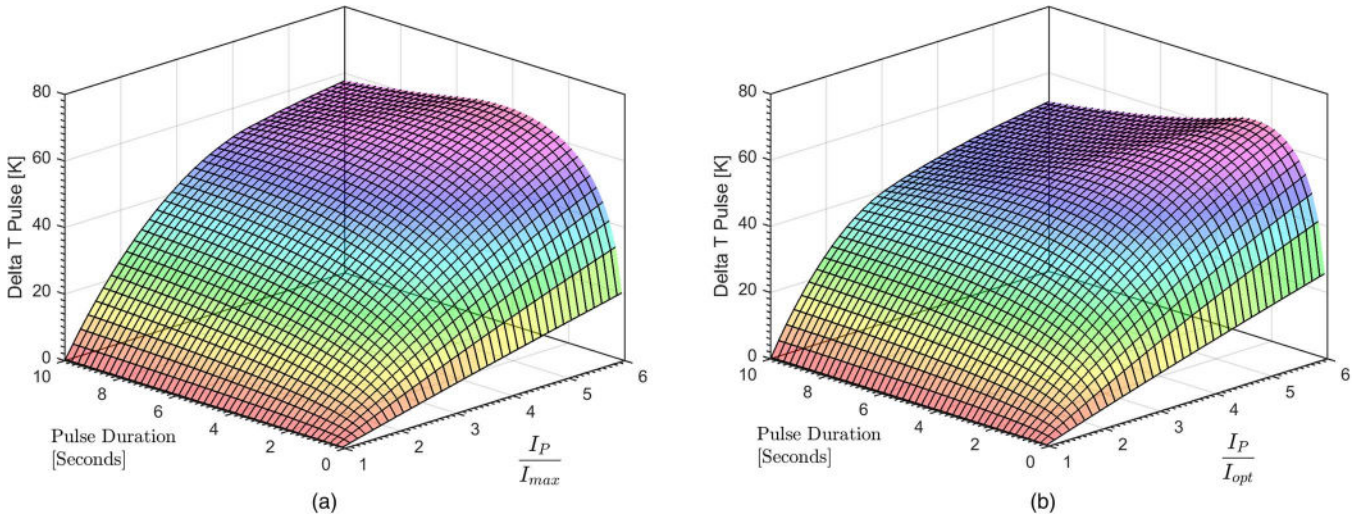


**Figure 4.** $\Delta T_{\text{Pulse}}$ (a) $I_{\text{max}}$ (b) $I_{\text{opt}}$.

Currently the SPICE model used herein only simulates the thermoelements. The accuracy of the SPICE model could be improved when using intrinsic properties by taking into account temperature dependent thermoelement material properties as this has been shown to have a significant effect.[31] Additional accuracy could be gained by adding thermal resistances of solder and copper, their masses, any thermal interface resistances[17] between the copper and heat sinks, the thermal resistance of heat sinks as well as the heat sink mass. If the heat sink is actively cooled, the heat transfer from the heat sink should be included. Further improvements could be gained by modeling the Joule heat generated within the solder and copper as well as radiative and convective losses.[27] To produce a model that accurately reproduces the transient effect from experimental data with intrinsic properties, these items must be included and / or provided in the experimental technical paper that provides experimental data. To simplify reporting, sometimes, $T_h$ is measured and reported vs. time and then imposed on the model.[42]. Additionally, it has be found[21] that 1 to 5 significant figures should be used when reporting parameters in order to reproduce transient supercooling results to one decimal place accuracy. Since this number varies, 5 significant figures is recommended for communicating these parameters.

## Response of Freestanding Couple to Pulsed Current

Response surfaces were created for each of the parameters that describe pulse cooling in Figure 1. The independent variables for the response surfaces are pulse duration and pulse height. All surfaces were generated using isosceles triangle shaped pulses. For each parameter, a surface was generated starting pulses from $I_{max}$ and another surface generated starting from $I_{opt}$ for comparison.

***$\Delta T_{Pulse}$.***—$\Delta T_{Pulse}$ is the difference between the steady state $T_c$ temperature and the minimum temperature achieved during the current pulse. This temperature difference is due to the difference in time constants between Joule heat and Peltier cooling.

In Figure 4, there is a clear maximum on both $\Delta T_{Pulse}$ surfaces. A clear trend is $\Delta T_{Pulse}$ is always higher with increasing $I_{\text{P}}/I_{\text{max}}$. It is also seen that in general $\Delta T_{\text{Pulse}}$ increases with longer pulse duration except for the highest $I_{\text{P}}/I_{\text{max}}$ values where it decreases. This reduction in $\Delta T_{\text{Pulse}}$ is due to the triangular shape of the pulse and interaction between Peltier cooling and Joule heat. The longer the duration of the Isosceles triangular pulse, the slower the ramp rate of current during the pulse. In the absence of Joule heat, the peak rate of heat removal at $T_c$ would be achieved at the peak of the current pulse since Peltier cooling linearly increases with current. For longer pulses, this peak heat removal would occur later. Now adding Joule heat back in, the time delayed Joule heat may reach $T_c$ before the Peltier cooling peaks at maximum current. In this way, for longer pulses, peak $\Delta T_{Pulse}$ is reduced. This does not happen at lower $I_{\text{P}}/I_{\text{max}}$ because Joule heat is dependent on the square of current.

***Pulse cooling enhancement.***—Pulse cooling enhancement is the ratio of $\Delta T_{Pulse}$ to $\Delta T_{max}$. A pulse cooling enhancement of 0.4 means a 40% reduction in temperature from the pulse compared to $I_{\text{max}}$ steady state operation. In Figure 5, a pulse cooling enhancement of 55% is seen with pulses starting from $I_{max}$ and slightly less for $I_{opt}$ of around 52%. The shape of this surface is the same as $\Delta T_{Pulse}$ because the same data is used for both surfaces. Value is added by presenting this data from two different perspectives. $\Delta T_{Pulse}$ is the perspective of absolute temperature and pulse cooling enhancement gives a normalized perspective that is useful when comparing between multiple independent experiments.

***Time to minimum temperature.***—Time to minimum temperature is the time at which $\Delta T_{Pulse}$ occurs. Time to minimum temperature in Figure 6 is the longest when pulse duration is maximum and $I_{\text{P}}/I_{\text{max}}$ is minimum. Time to minimum temperature is the minimum with minimum pulse duration throughout the range of pulse-heights. The two surfaces of Figure 6 are very similar with exception of the area in the upper right hand corner where a transition occurs. In this area it appears that time to minimum temperature decreases nonlinearly with increasing $I_{\text{P}}/I_{\text{max}}$ and decreases linearly with increases pulse duration. For shorter pulses, there is no non-linear reduction with $I_{\text{P}}/I_{\text{max}}$. The reason for this has to do with the time separation of Peltier cooling and Joule heat and the slope current vs. time. For shorter pulses, the pulse and minimum temperature occur before Joule heat has time reach $T_c$ and slow down the decrease to minimum temperature. For longer pulses, the Joule heat reaches $T_C$ before the Peltier cooling can peak at the apex of the triangular pulse. It takes much longer to reach the current apex for a long duration triangle.

Shorter pulses reach minimum temperature sooner because the peak current and thus peak Peltier cooling is reached faster due to the current pulse shape. If peak Peltier cooling is reached sooner, time to minimum temperature is shorter. There is a linear trend of decreasing time to minimum temperature with increased $I_{\text{P}}/I_{\text{max}}$ at constant pulse duration at the lower end of pulse duration range. This happens because the heat removed from $T_c$ in Joules is substantially proportional to the rate in watts at which it is removed. With higher $I_{\text{P}}/I_{\text{max}}$, the minimum temperatures get lower, however the cooling rate is faster than for lower $I_{\text{P}}/I_{\text{max}}$. This keeps the time to minimum temperature about the same throughout the range of $I_{\text{P}}/I_{\text{max}}$. The linear trend is more pronounced at short pulse durations because time

Redistribution subject to ECS terms of use (see ecsdl.org/site/terms_use) unless CC License in place (see abstract).

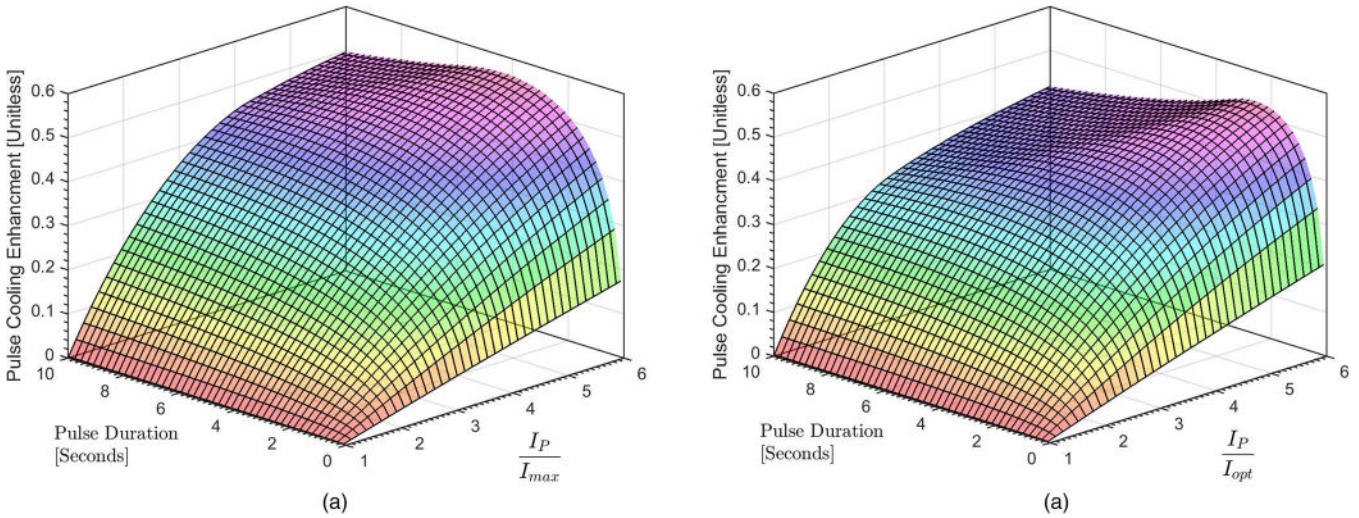


**Figure 5.** Pulse Cooling Enhancement (a) $I_{\max}$ (b) $I_{\text{opt}}$.

delayed Joule heat is less of a factor for short pulses. The pulses are complete before the Joule heat arrives.

The area of decreased time to minimum temperature in the upper right corner is larger for the $I_{opt}$ current because of operation at a higher current. The effects are magnified due to more Joule heat.

***Holding time.***—Holding time is defined as the amount of time during a transient pulse event that $T_c$ spends below steady state temperature. Figure 7 shows holding time is a linear function of pulse duration and a nonlinear function of $I_{\text{P}}/I_{\max}$. Although not shown on Figure 7a for clarity, for $I_{\max}$ operation and $I_{\text{P}}/I_{\max}$ smaller than 1.146, holding time increases to approximately 300 to 400 seconds with pulse duration ranging from 0.1 to approximately 10 seconds. Peak holding time for $I_{\max}$ operation is much higher than that of $I_{\text{opt}}$ operation.

The nonlinear decrease in holding time is due to an exponential amount of Joule heat relative to Peltier cooling. Peltier cooling increases linearly with increased current and Joule heat increases with the square of current. The increased heat reaching $T_c$ reduces the time spent below steady current operation.

***Transient advantage.***—Transient advantage is the area of the supercooling portion of a transient pulse event. This metric is an aggregate of both minimum temperature achieved and time spent below $I_{\max}$ steady state temperature which is also known as holding time. Transient advantage is illustrated by the purple shaded area in Figure 1. The peak transient advantage is the point that has the best combination of minimum temperature achieved and longest holding time.

From Figure 8 the effects of both pulse duration and $I_{\text{P}}/I_{\max}$ are nonlinear. The maximum transient advantage occurs at approximately $I_{\text{P}}/I_{\max} = 4$ for both $I_{\max}$ and $I_{\text{opt}}$. Additional transient advantage may be gained with additional pulse duration that is beyond the independent variable limits studied here. The peak transient advantage is around $225Ks$ for $I_{\max}$ operation and around $175Ks$ for $I_{\text{opt}}$ operation.

$\boldsymbol{\Delta T_{post\ pulse}}$.—$\Delta T_{\text{postpulse}}$ is the magnitude of the delta between the maximum temperature achieved and the temperature achieved by steady state operation. In Figure 9, we see that $\Delta T_{\text{postpulse}}$ increases linearly with pulse duration and exponentially with $I_{\text{P}}/I_{\max}$. For pulses starting from $I_{max}$ operation, $\Delta T_{\text{postpulse}}$ was 150 K versus 300 K for pulses starting from $I_{opt}$ when influenced by the same independent variables.

Temperature is a function of heat added in Joules to $T_c$. More heat added to $T_c$ increases its temperature. Increasing $I_{\text{P}}/I_{\max}$ exponentially increases Joule heat added to $T_c$ due to Joule heating being proportional to the square of current. The linear increase in $\Delta T_{\text{postpulse}}$ with

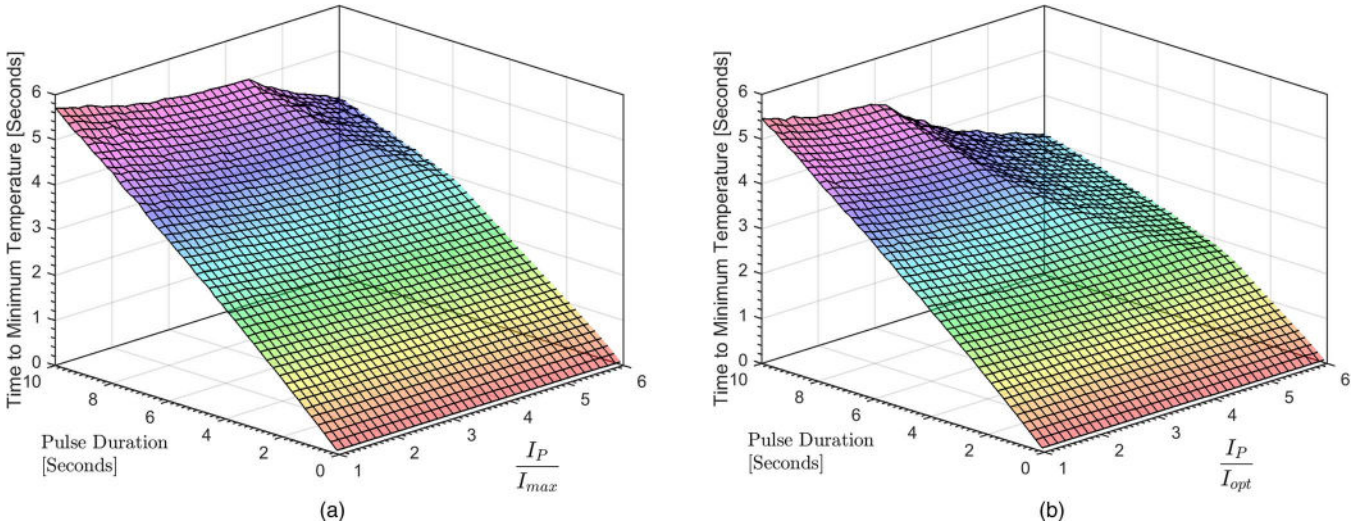


**Figure 6.** Time to Minimum Temperature (a) $I_{\max}$ (b)$I_{\text{opt}}$.

Redistribution subject to ECS terms of use (see ecsdl.org/site/terms_use) unless CC License in place (see abstract).

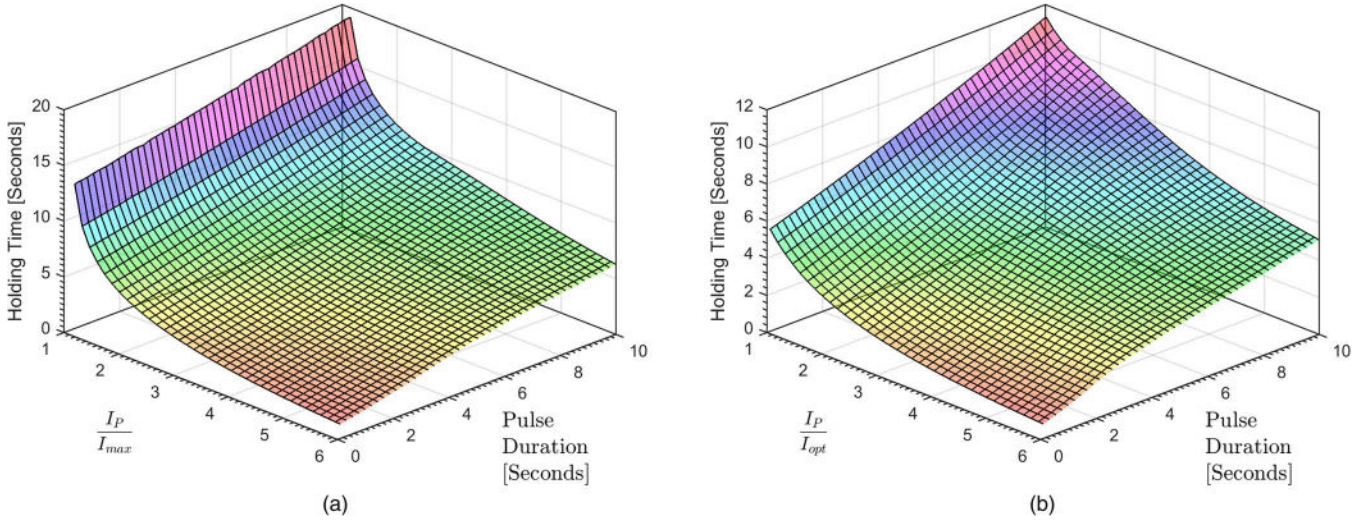


**Figure 7.** Holding Time (a) $I_{\max}$ (b) $I_{\text{opt}}$.

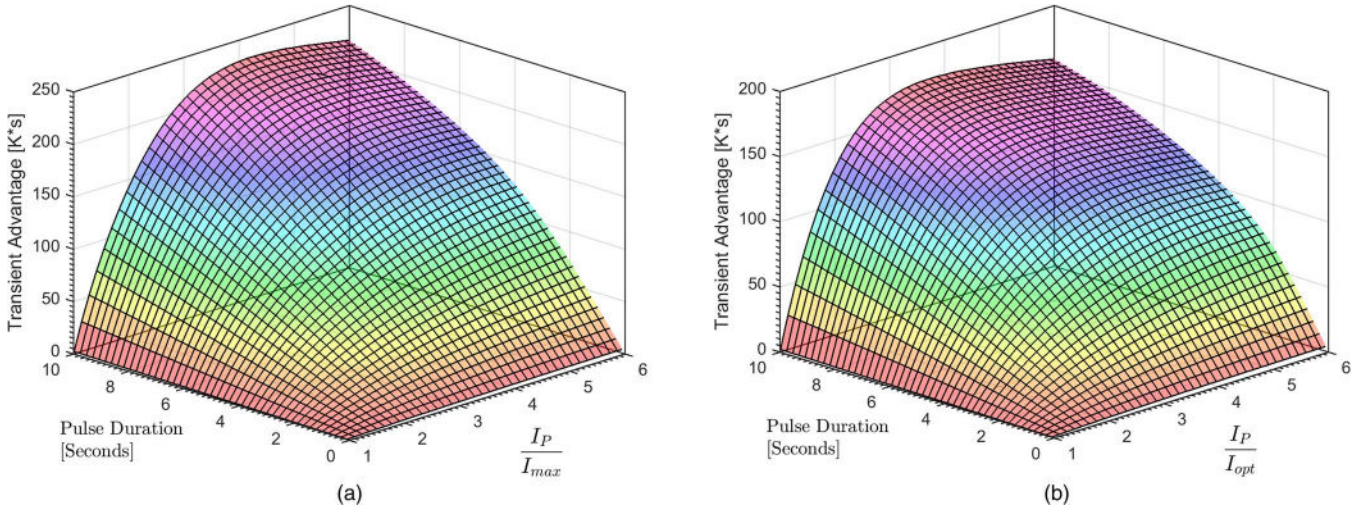


**Figure 8.** Transient Advantage (a) $I_{\max}$ (b) $I_{\text{opt}}$.

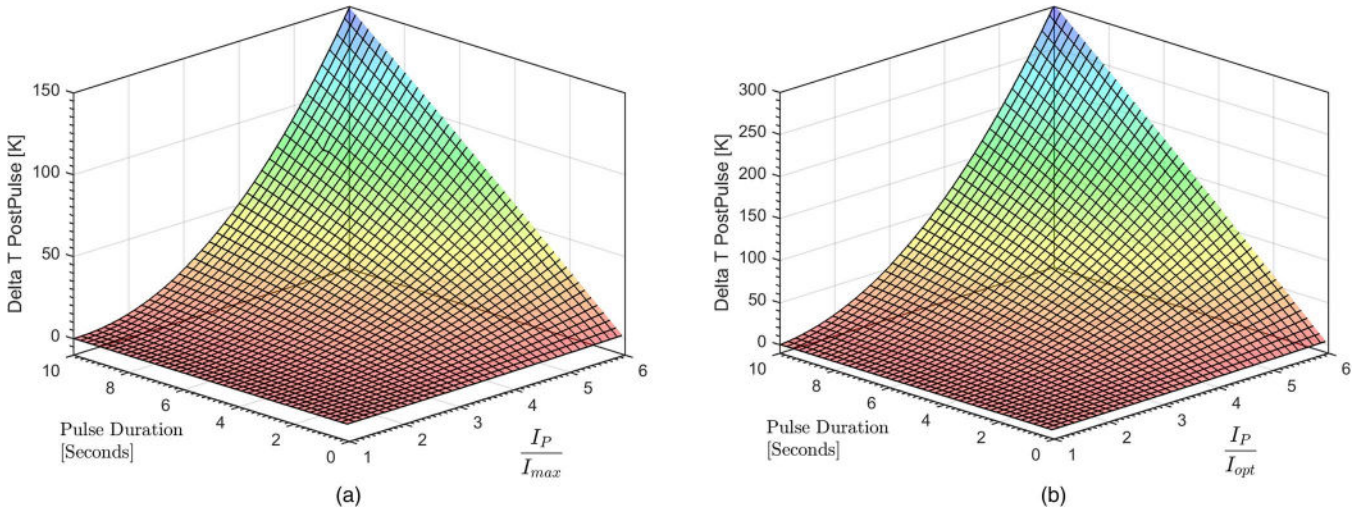


**Figure 9.** $\Delta T_{\text{post pulse}}$ (a)$I_{\max}$ (b) $I_{\text{opt}}$.

Redistribution subject to ECS terms of use (see ecsdl.org/site/terms_use) unless CC License in place (see abstract).

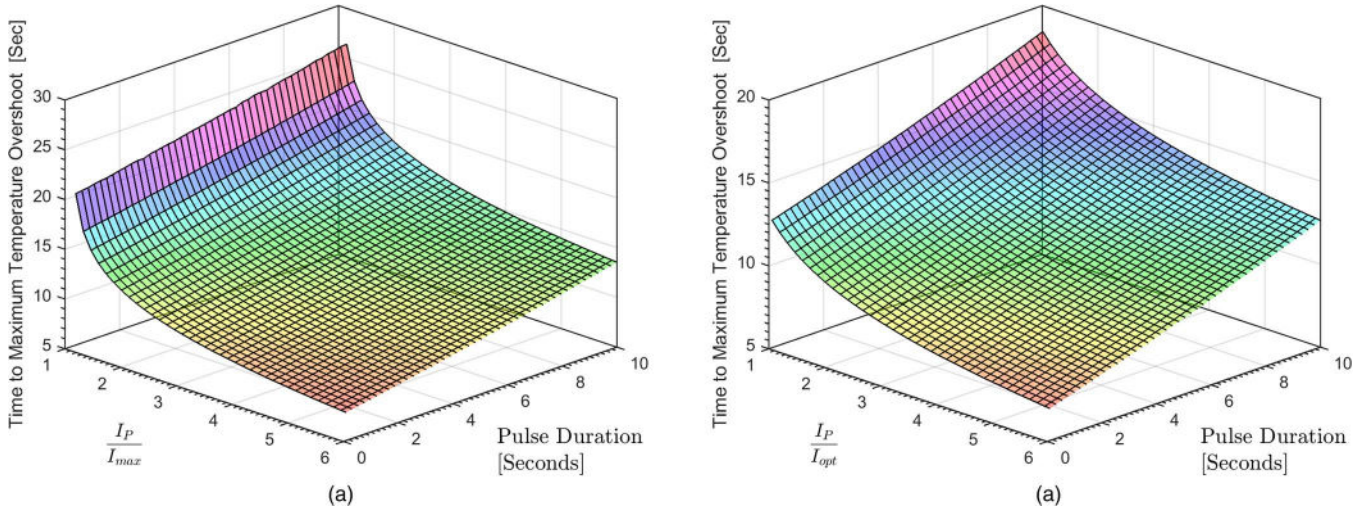


**Figure 10.** Time to Maximum Temperature (a) $I_{\max}$ (b) $I_{\text{opt}}$.

increased pulse duration is due to a linear increase in heat added to $T_c$. With the same $I_P/I_{\max}$, the rate of Joule heat generation is the same from one pulse duration to the next, however the duration increases. The total heat addition is the power multiplied by the duration. This heat added is linearly proportional to pulse duration and thus we see the linear trend.

***Time to maximum temperature overshoot.—***Time to maximum temperature overshoot is the time to maximum temperature during the transient pulse event. This maximum temperature can occur after or during the pulse, depending on the pulse duration. In Figure 10 the time to maximum temperature overshoot is a linear function of pulse duration and a nonlinear function of $I_P/I_{\max}$. The maximum time to maximum temperature occurs at maximum pulse duration and minimum $I_P/I_{\max}$. The minimum time to maximum temperature overshoot occurs at the shortest pulse duration and largest $I_P/I_{\max}$. For the same range of independent variables, the time to maximum temperature overshoot is longer starting from $I_{\max}$ than from $I_{\text{opt}}$.

Time delayed Joule heat is responsible for the maximum temperature overshoot. The time required to get to maximum temperature overshoot is highly dependent on the rate at which Joule heat is being generated and the time the maximum temperature overshoot begins. Higher $I_P/I_{\max}$ generates Joule heat at an exponential rate compared to Peltier cooling. This results in the nonlinear decrease in time to minimum temperature at higher $I_P/I_{\max}$. The linear decrease in time to minimum temperature with decreasing pulse duration is due to the linear reduction in heat in Joules added to $T_c$ due to a linear reduction in duration for which that heat is generated. Since the overshoot cannot occur until after holding time, longer holding means a longer wait for maximum temperature overshoot. This longer wait is proportional to the increase in pulse duration.

***Transient penalty.—***Transient penalty is the area of the superheating portion of a transient pulse event. This metric is an aggregate of $\Delta T_{\text{post pulse}}$ and settling time. Transient penalty is illustrated by the green shaded area in Figure 1. In Figure 11, the transient penalty increases linearly with pulse duration and exponentially with $I_P/I_{\max}$. Transient penalty approaches zero at very small pulse height and pulse duration.

At constant pulse duration and higher $I_P/I_{\max}$, the rate of Joule heat generation is exponentially higher. $\Delta T_{\text{postpulse}}$ increases because more Joules of heat have been added to $T_c$. Heat is added at the same rate for a constant $I_P/I_{\max}$ however more pulse duration linearly adds heat in Joules to $T_c$. This is why the linear trend with pulse duration is seen.

***Net transient advantage.—***Net transient advantage is the difference between transient advantage and transient penalty. A positive

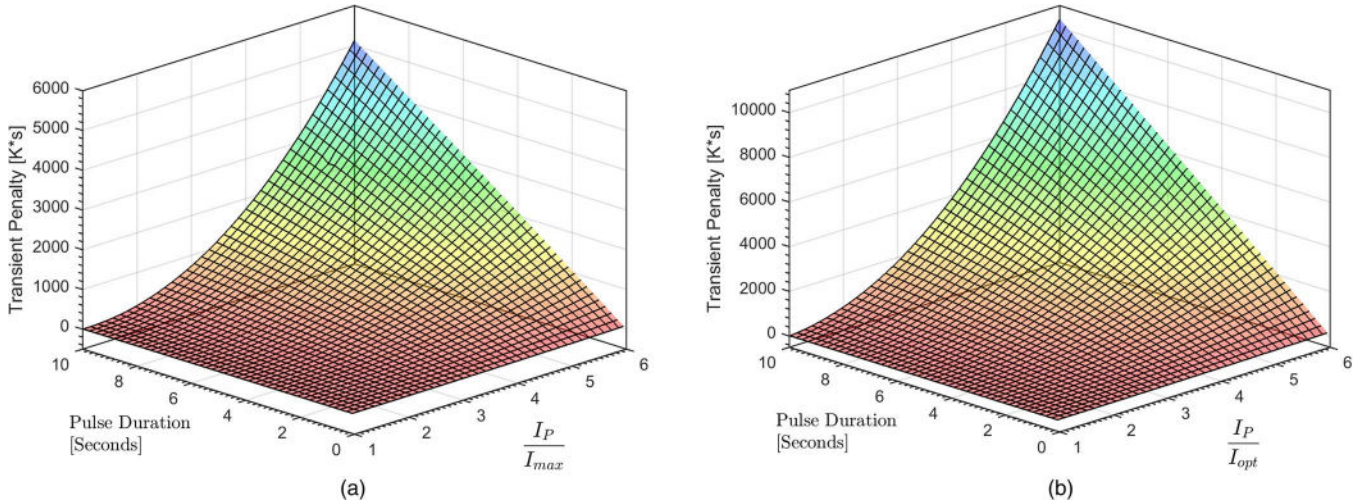


**Figure 11.** Transient Penalty (a) $I_{\max}$ (b) $I_{\text{opt}}$.

Redistribution subject to ECS terms of use (see ecsdl.org/site/terms_use) unless CC License in place (see abstract).

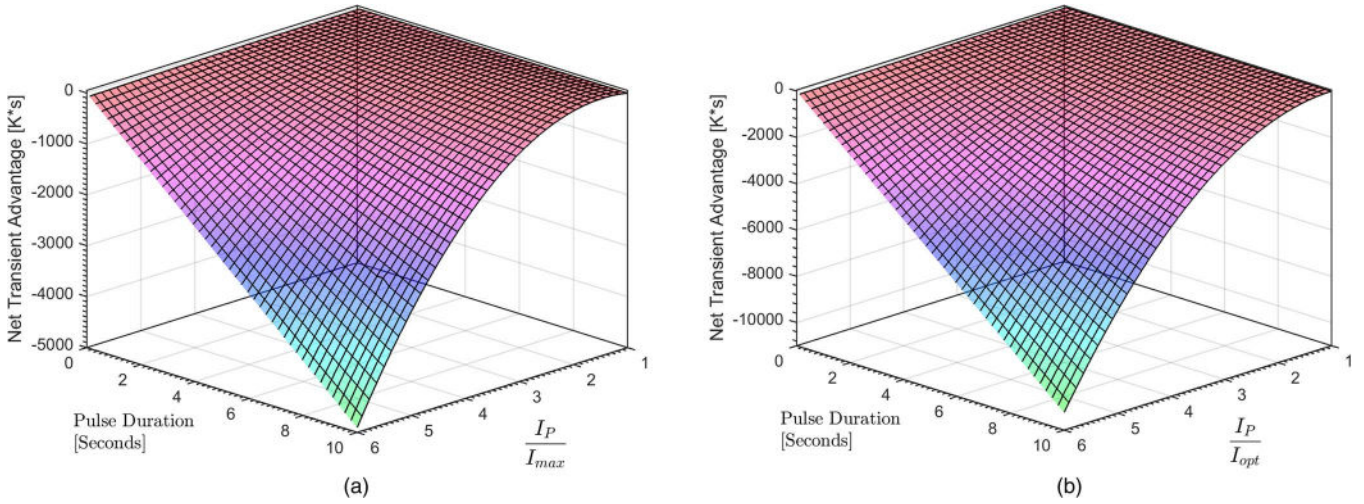


**Figure 12.** Net Transient Advantage - Full Study Range Surface (a) $I_{max}$ (b) $I_{opt}$.

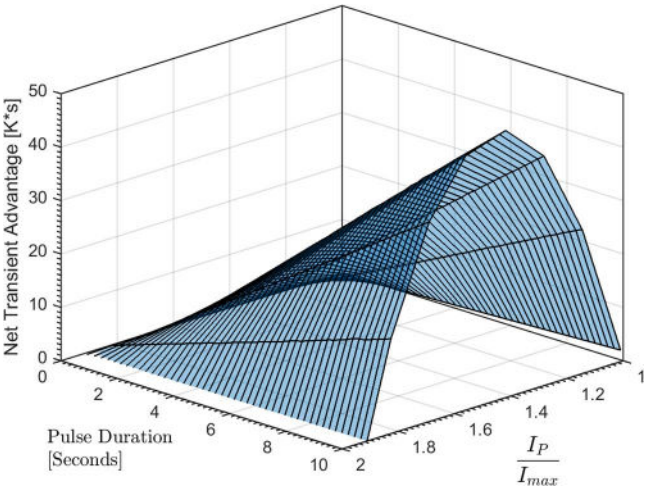


**Figure 13.** Net Transient Advantage - Advantage Portion, $I_{max}$ Surface.

difference is a net advantage or net cooling and a negative difference is a net penalty or net heating. A net advantage indicates a net increase in $Q_c$ for a transient pulse event over steady state operation. From Figure 12, for both $I_{max}$ and $I_{opt}$ operation, net transient advantage appears to approach zero. Upon closer inspection of the $I_{max}$ operation surface and magnifying the scale, a net advantage is found. In Figure 13, this net transient advantage become more apparent. It is seen that $I_{max}$ operation contains a net advantage between an $I_P/I_{max}$ of 1 and 2. The net transient advantage also increases with pulse duration. Figure 14 shows the same data as the two surfaces in Figure 12. The figures are now viewed from the side and without surface. Figure 14 clearly shows the area where $I_P/I_{max}$ creates a net transient advantage for $I_{max}$ operation and the same $I_P/I_{max}$ for $I_{opt}$ creates a net transient penalty.

## Conclusions

A single freestanding thermocouple was one-dimensionally modeled using electric-thermal analogies and solved for transient response using SPICE software. For the first time, response surfaces were

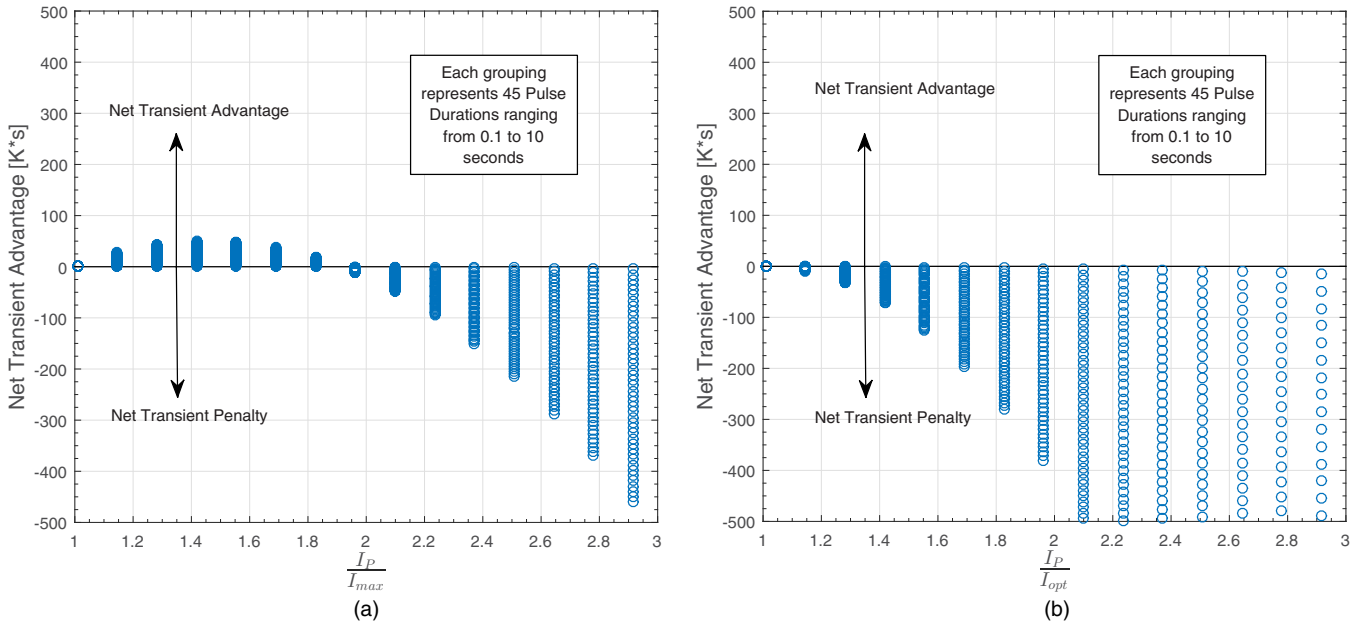


**Figure 14.** Net Transient Advantage - Partial Study Range, Alternate View (a) $I_{max}$ (b) $I_{opt}$.

Redistribution subject to ECS terms of use (see ecsdl.org/site/terms_use) unless CC License in place (see abstract).

generated for the dependent variables relevant to Peltier pulse cooling. The results indicate the combination of pulse duration and pulse height that can maximize Net Transient Advantage for an Isosceles shaped current pulse. Additionally, a systematic parametric study to find optimums and trade-offs for each dependent variable was completed. For current pulses starting from $I_{max}$ a Net Transient Advantage exists. When starting from from $I_{opt}$, however, no Net Transient Advantage was found. For very low pulse heights a Transient Advantage can exist with no Transient Penalty. For pulse cooling, this fulfills the iNEMI roadmap goal of finding more effective and cost efficient ways of removing heat from electronic systems.

The results of the simulation indicate an optimum combination of pulse height and duration. This optimum combination varies depending upon the dependent variable. The method of using response surfaces is well-suited to comparing different pulse shapes on a common basis. It is possible that the optimum dependent variable values are the same for any given pulse shape, but occur at different combinations of independent variable for the same energy input. A future study could investigate other types of current pulse shapes.

## References


1. G. O'Malley, Highlights from the inemi thermal management technology roadmap, 2014.
2. L. Technologies, Thermoelectric handbook, 2014.
3. Hot spot cooling using embedded thermoelectric coolers, 22nd IEEE SEMI-THERM Symposium, 2006. doi:1109/STHERM.2006.1625219.
4. TECA, Thermoelectric air conditioner applications, 2015.
5. Kryotherm, Thermoelectric coolers for domestic cooling devices, 2015.
6. Gentherm, Our revolutionary climate control sleep system (ccss), 2015.
7. Gentherm, Personalized microclimate technology, 2015.
8. Thermotek, Medical devices, Website, 2015.
9. Gentherm, Climate seats, 2015.
10. Gentherm, Thermal convenience, 2015.
11. T. Barnhart, A. Piggott, D. Kossakovski, and K. Smith, Distributed battery thermal management using thermoelectrics, 2014. SAE Thermal Management Symposium.
12. A. Piggott, D. Kossakovski, and T. Barnhart, Thermoelectric based thermal management system, 2015.
13. Improving efficiency of a vehicle HVAC system with comfort modeling, zonal design, and thermoelectric devices, Deer Conference, 2012.
14. D. Mitrani, J. Salazar, A. Turi, M. J. Garcia, and J. A. Chavez, Transient distributed parameter electrical analogous model of te devices, *Microelectronics Journal*, **40**, 1406 (2009).
15. G. J. Snyder, J.-P. Fleurial, T. Caillat, R. Yang, and G. Chen, Supercooling of peltier cooler using a current pulse, *Journal of Applied Physics*, **92**, 1564 (2002).
16. R. Yang, G. Chen, G. J, Ravi Kumar, A. Snyder, and J.-P. Fleurial, Transient cooling of thermoelectric coolers and its applications for microdevices, *Energy Conversion and Management*, (2005).
17. H. Lee, A. M. Attar, and S. L. Weera, Performance prediction of commercial thermoelectric cooler modules using the effective material properties, *Journal of Electronic Materials*, **44**, 2157 (2015).
18. S. Lineykin and S. Ben-Yaakov, Analysis of thermoelectric coolers by a spice-compatible equivalent-circuit model, *IEEE Power Electronics* (2005).
19. M. Manno, W. Peng, and A. Bar-Cohen, Pulsed thermoelectric cooling for improved suppression of a germanium hotspot, Components, Packaging and Manufacturing Technology, *IEEE Transactions on*, **4**, 602 (2014).
20. M. V. Manno, ON-CHIP THERMOELECTRIC HOTSPOT COOLING, Ph.D. thesis, University of Maryland, 2015.
21. A. J. Piggott, Transient Thermoelectric Supercooling: Isosceles Current Pulses From a Response Surface Perspective And The Performance Effects Of Pulse Cooling a Heat Generating Mass, Master's thesis, Michigan Technological University, 2015.
22. O. A. Sullivan, Embedded Thermoelectric Devices For On-chip Cooling And Power Generation, Ph.D. thesis, Georgia Institute of Technology, 2012.
23. T. Thonhauser, G. D. Mahan, L. Zikatanov, and J. Roe, Improved supercooling in transient thermoelectrics, *Applied Physics Letters*, **85**, 3247 (2004).
24. O. Sullivan, M. P. Gupta, S. Mukhopadhyay, and S. Kumar, Thermoelectric coolers for thermal gradient management on chip, in: ASME 2010 International Mechanical Engineering Congress and Exposition, *American Society of Mechanical Engineers*, 187 (2010).
25. J. Mao, H. Chen, H. Jia, and X. Qian, The transient behavior of peltier junctions pulsed with supercooling, *Journal of Applied Physics*, **112**, 014514 (2012).
26. M. Redmond, K. Manickaraj, O. Sullivan, S. Mukhopadhyay, and S. Kumar, Hotspot cooling in stacked chips using thermoelectric coolers, Components, Packaging and Manufacturing Technology, *IEEE Transactions on*, **3**, 759 (2013).
27. H. Lv, X.-D. Wang, T.-H. Wang, and J.-H. Meng, Optimal pulse current shape for transient supercooling of thermoelectric cooler, *Energy*, **83**, 788 (2015).
28. M. Ma, J. Yu, and J. Chen, An investigation on thermoelectric coolers operated with continuous current pulses, *Energy Conversion and Management*, **98**, 275 (2015).
29. G. E. Hoyos, K. Rao, and D. Jerger, Fast transient response of novel peltier junctions, *Energy Conversion*, **17**, 45 (1977).
30. Geometric Effects on the Transient Cooling of Thermoelectric Coolers, volume 691, Boston, Massachusetts, U.S.A., 2001.
31. H. Lv, X.-D. Wang, and C.-H. Wang, Tian-Huand Cheng, Improvement of transient supercooling of thermoelectric coolers through variable semiconductor cross-section, *Applied Energy* (2016).
32. H. Lv, X.-D. Wang, J.-H. Meng, T.-H. Wang, and W.-M. Yan, Enhancement of maximum temperature drop across thermoelectric cooler through two-stage design and transient supercooling effect, *Applied Energy*, (2016).
33. Melcor, Melcor thermal solutions, Not Listed. Emailed from Daniel Mitrani.
34. Finite Elements for Thermoelectric Device Analysis in ANSYS, 2005. 2005 International Conference on Thermoelectrics.
35. M. Jaegle, Multiphysics simulation of thermoelectric systems - modeling of peltier-cooling and thermoelectric generation, Excerpt from the Proceedings of the COMSOL Conference 2008 Hannover (2008).
36. L. W. Nagel and D. O. Pederson, SPICE (Simulation Program with Integrated Circuit Emphasis), Technical Report, University of California, Berkele, 1973.
37. J. A. Chavez, J. A. Ortega, J. Salazar, A. Twb, and M. Garcia, Spice model of thermoelectric elements including thermal effects, IEEE (2000). There was no journal listed.
38. Spice Compatible Equivalent Circuit of the Energy Conversion Process in Thermoelectric Modules, 2004.
39. O. Sullivan, B. Alexandrov, S. Mukhopadhyay, and S. Kumar, 3d compact model of packaged thermoelectric coolers, *Journal of Electronic Packaging*, **135**, 031006 (2013).
40. P. D. Mitcheson, Spice algorithms and internals, Web, 2006.
41. Melcor, Thermoelectric handbook, Unknown.
42. N. Q. Nguyen and K. V. Pochiraju, Behavior of thermoelectric generators exposed to transient heat sources, *Applied Thermal Engineering*, **51**, 1 (2013).


Redistribution subject to ECS terms of use (see **ecsdl.org/site/terms_use**) unless CC License in place (see abstract).